2.2. X-Ray Tomography (XRT) and Real-Time Radiography (RTR) Techniques

Sandia has very extensive radiographic facilities for determining material distribution. These facilities have generally been applied to solid objects in the past, but application to flowing systems is possible as well under certain circumstances. Two different systems were used to perform validation experiments (Thompson and Stoker, 1997). One was an x-ray tomography (XRT) system for performing tomographic reconstructions of static material distributions, and the other was a real-time radiography (RTR) system capable of providing a temporally resolved x-ray "shadow" of a flow.

2.2.1. XRT System

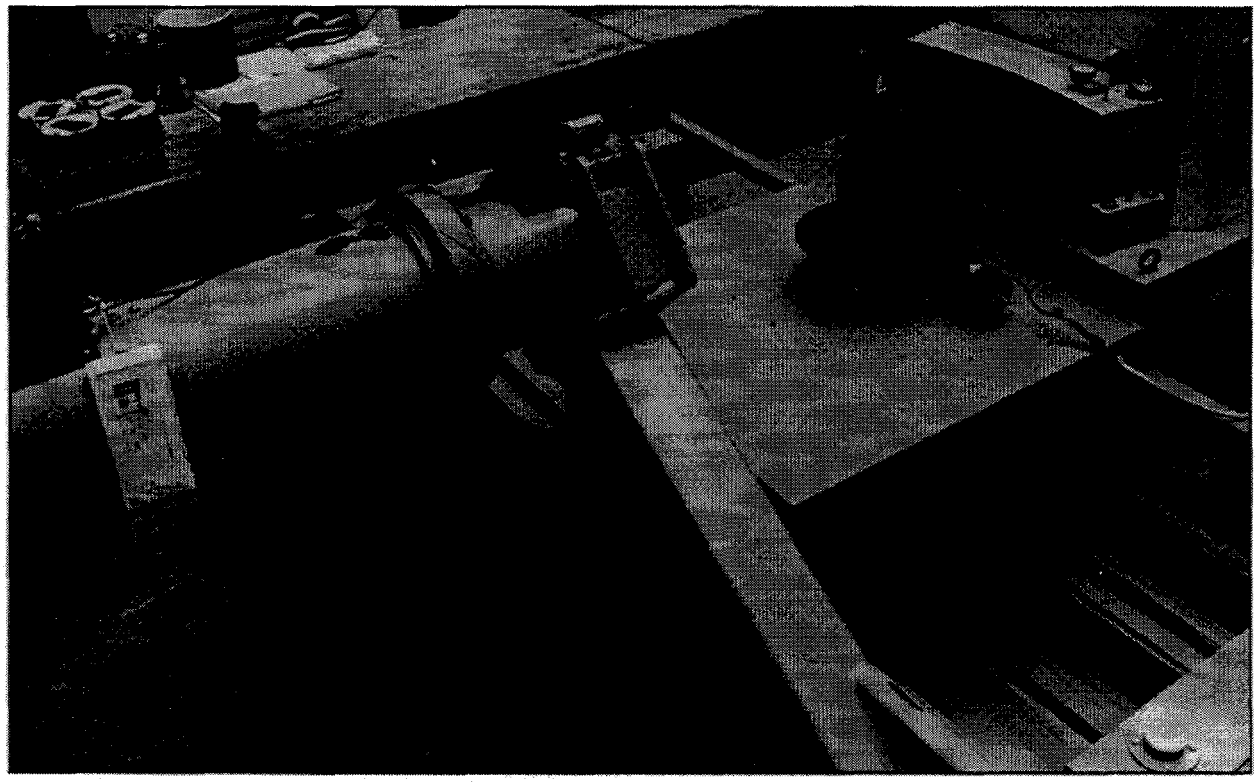

Figure 11. X-ray tomography (XRT) experimental setup.

The XRT system, shown in Figure 11, employs a Van de Graaff accelerator (at left of Figure 11) weighing approximately 2000 kg to produce a beam of x-ray photons with energies up to 2 MeV. A 31-channel Scientific Measurement Systems coplanar detector array (at right of Figure 11) of NE102 plastic scintillators bonded to photomultiplier tubes (PMTs) is used to detect the x-ray photons transmitted through the object to be imaged. This detector array is capable of being laterally repositioned (dithered) to 20 stations to create a much larger virtual array with $31 \times 20 = 620$ detectors. A thresholded pulse-counting approach is used to record the x-ray photons for each detector.

Objects with diameters up to 1 m and weights up to 200 kg can be placed on the translational-rotational stage between the x-ray source and the detector array (at center of Figure 11). Each combination of a translational position and a rotational position constitutes a projection. For objects fitting within the angular width of the detector array, a scan may involve acquiring x-ray counts for the 620 virtual detectors (i.e. for 620 "rays" per projection) at 360 angular positions (360 projections). For larger objects, some translations may be also required. Acquiring a full data set (620 virtual detectors, 360 projections) for imaging one slice through an object requires about 2.5 hours.

A standard filtered back-projection algorithm is used to perform the tomographic reconstruction for the XRT system (cf. Herman, 1983; Howard, 1985). For the full data set indicated above, this method yields a resolution of about 1-2 line pairs per millimeter (a spatial resolution of about 0.25-0.50 mm).

2.2.2. RTR System

The RTR system employs a Pantak x-ray machine capable of producing x-ray photons with energies up to 0.3 MeV. These x-rays pass through the object and are incident on a gadolinium oxysulfide bare-phosphor screen, which is imaged using a RS170 intensified CCD camera at the standard video frame rate. The field of view for this system is the standard $14 \text{ inch} \times 17 \text{ inch}$ ($35.6 \text{ cm} \times 43.2 \text{ cm}$). No translation or rotation stages are routinely present for this system.

2.3. Gamma-Densitometry Tomography (GDT) Technique

One method of characterizing the phase volume fraction spatial variation is gamma-densitometry tomography (GDT). The basic physics of the interaction of gamma photons with matter is well known (cf. Meyerhof, 1967; Lapp and Andrews, 1972; Knoll, 1979; Lamarsh, 1983). In brief, there are three interaction mechanisms: the photoelectric effect, pair production, and Compton scattering. The first two are absorptive (the gamma photon disappears), whereas the last one is not (the energy and direction of the gamma photon change). These processes cumulatively yield a mass attenuation coefficient μ/ρ (units of cm^2/g), a constant depending only on the composition of the material and the gamma photon energy. The attenuation coefficient μ, roughly proportional to the electron density of the medium for the lighter elements and the gamma photon energies considered here, describes the attenuation of a gamma beam of intensity I passing along a path of length L through the material:

$$I = I_0 \exp(-\mu L) . \tag{8}$$

If two or more materials are present along the path, a measurement of I/I_0 yields the average attenuation coefficient μ along the path, where the value of μ is linearly related to the volume fractions ε_i and their attenuation coefficients μ_i of the materials comprising the mixture:

$$\mu = \sum_i \varepsilon_i \mu_i , \text{ where the } \varepsilon_i \text{ are averaged over the path } L . \tag{9}$$

Measuring μ in this manner along many different paths provides the information needed to perform a tomographic reconstruction of the spatial variation of μ. The varieties of tomographic reconstruction algorithms which accomplish this are discussed in great detail elsewhere (e.g. Herman, 1983; Howard, 1985; Vest, 1985). If only two materials are present, the volume fraction spatial distribution of each material can be uniquely determined since the two volume fractions must sum to unity.

Investigators have long recognized the potential of GDT to study multiphase flows. A comprehensive review discussing applications of GDT to multiphase flows is provided by Munshi (1990). Typical

applications have included two-phase gas-liquid pipe flows for the nuclear industry (Hewitt, 1978), saturation measurements in porous media (Reda et al., 1981; Brown et al., 1993), gas-solid fluidized beds (MacCuaig et al., 1985; Dyakowski, 1996), gas-liquid flow in packed beds (Toye et al., 1996), particle-laden liquid flows (Shollenberger et al., 1997b), horizontal stratified three-phase pipe flow (Pan and Hewitt, 1995), and bubble columns (Kumar et al., 1995; Shollenberger et al., 1995ab; Adkins et al., 1996; Shollenberger et al., 1997a; Torczynski et al., 1995; Torczynski et al., 1996ac).

2.3.1. GDT System

The GDT system developed for this study is shown in Figure 12. It consists of a gamma source, a gamma detector, a multichannel analyzer for recording the gamma energy spectrum, a traverse for the source and detector, a PC for data acquisition, and software for count-rate analysis.

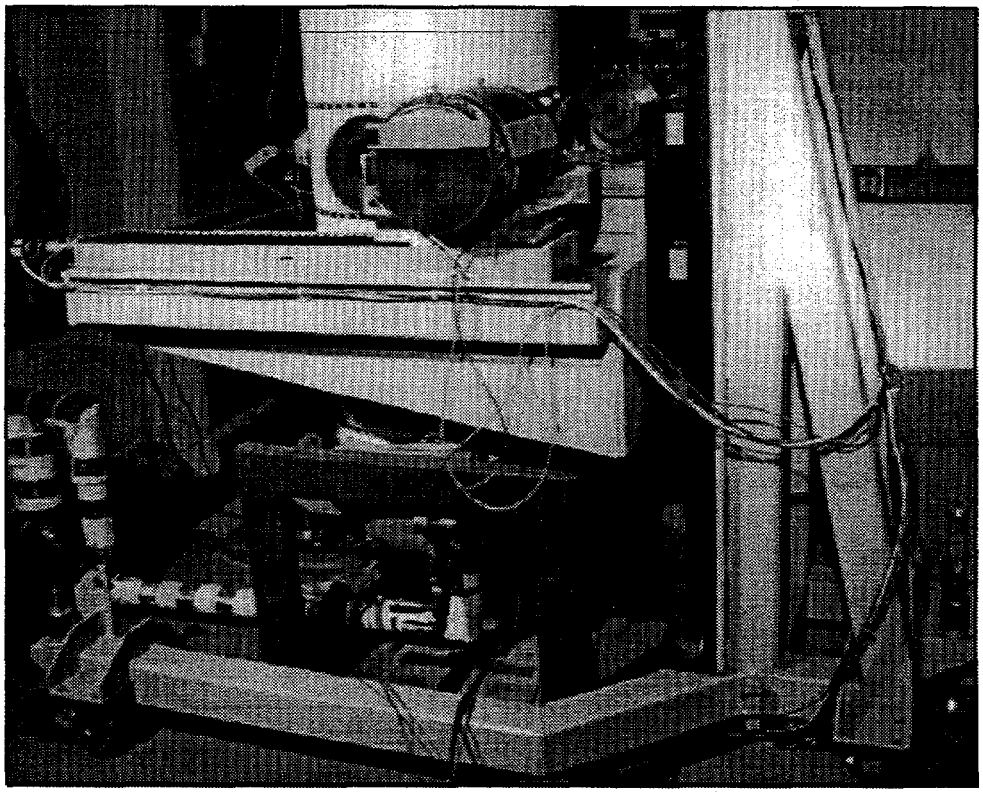

Figure 12. Gamma-densitometry tomography (GDT) system.

The gamma source used in the GDT system is a 5-Curie ^{137}Cs (cesium 137) isotope source. This isotope is fairly stable, having a half-life of roughly 30 years, and produces a fairly monoenergetic spectrum of gamma photons centered on 661.6 keV. The source is contained in a thick-walled cylindrical lead vault for safety purposes. A collimated beam is produced using a small-diameter aperture, for which diameters of 3.66 mm and 6.35 mm have been employed to date. The source is fully interlocked with an infrared sensor that activates the aperture-closure mechanism should a human be detected by the sensor. The aperture-closure mechanism has been designed to require a continual supply of power to remain open so that gravity-driven closure occurs if power is interrupted.

A scintillation detector is used to observe the individual gamma photons that pass through the scanned object without being scattered. The scintillation detector employs sodium iodide with thallium activator, NaI(Tl), in the form of a cylindrical crystal 7.62 cm in diameter and 7.62 cm long. The crystal is optically coupled to a photomultiplier tube (PMT) so that the flashes of light produced by individual photons can be observed. The detector crystal is water-cooled with active control to provide temperature stability and minimize thermal drift of the electronics. It is possible for gamma photons that are scattered by the scanned object to enter the detector, creating a spurious signal (see Figure 13). To minimize spurious acquisition of gamma photons that have been scattered through small angles, the detector is lead-shielded and a small-diameter aperture (3.66 mm or 6.35 mm) is placed in front of the detector to provide angular selectivity. The apertures on the source and detector also serve to collimate the gamma beam and thereby restrict the lateral extent of the region sampled by the source-detector combination for a particular position.

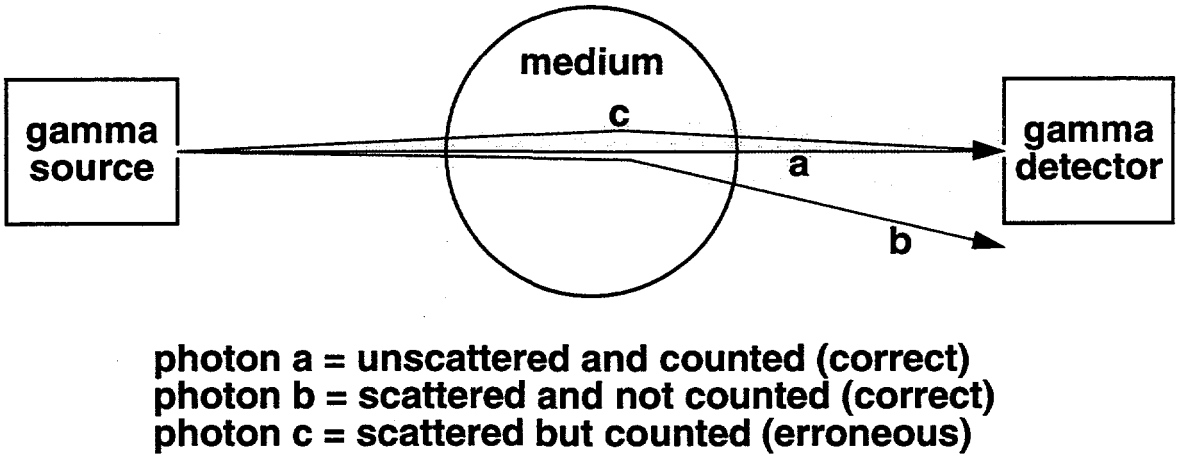

Figure 13. A detector erroneously observes some of the scattered gamma photons.

A heavy-duty computer-controlled two-axis traverse, shown schematically in Figure 14, is used to support, align, and position the source and the detector. The traverse is configured in a U-shape formed by two opposing arms, on which the source and the detector are mounted. The arms have 66 cm of clearance to accommodate large testbeds, and the traverse has 60 cm of travel in both the horizontal and the vertical directions. The U-shaped configuration allows the traverse system to be positioned easily around the testbed to be scanned and to be moved without difficulty from one testbed to another. The motion of the traverse is fully automated. A scan direction (vertical or horizontal), a step size (distance from one path to the next), and a time to collect counts are specified, and the traverse software automatically moves the source-detector combination to the correct position for the correct amount of time, where positions are determined by detection of positional changes in an encoder rotating with the traverse drive shafts. If a source-detector misalignment of more than 1 mm is detected, the gamma system is automatically shut down in the manner discussed above.

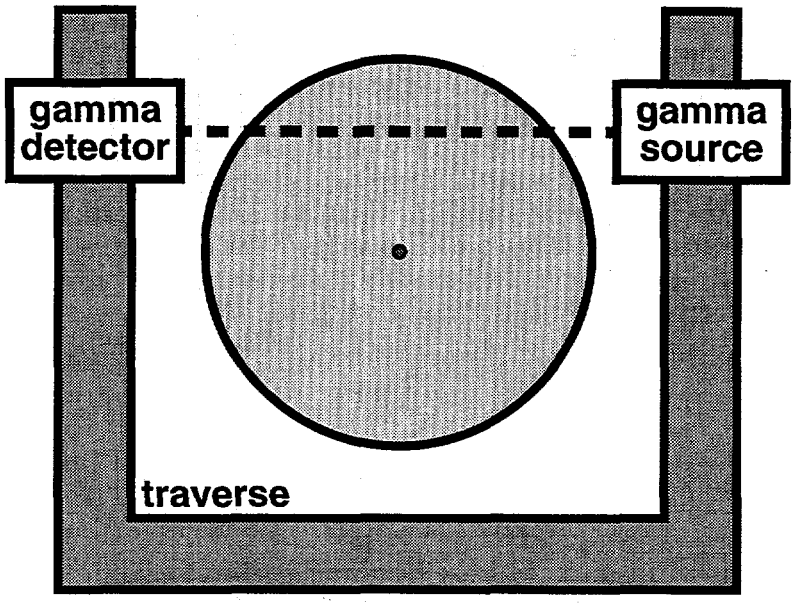

Figure 14. Schematic diagram of traverse for source and detector.

A multichannel analyzer (MCA) is used to measure the energy spectrum of the gamma photons so that the count rate can be determined. More accurately, the MCA measures the spectrum of the electrical pulses from the PMT that are produced by the light flashes from the sodium iodide crystal when gamma photons are incident on it. Typically, 720 contiguous bins are used to span the energy region from 0 to roughly 1400 keV. The MCA operates by acquiring data for a prescribed counting duration, the "live time". However, it requires a finite interval of time to record each count and cannot record additional counts that occur during those intervals, the "dead time". As a result, the total time needed to acquire a spectrum, the "wall-clock time", is somewhat longer than the live time. Calculations of count rates use the number of counts and the live time.

Some typical spectra observed with the MCA are shown in Figure 15. There are several distinguishing features on each of these curves that can be related to Compton-scattering phenomena and detector performance. First, the largest peak occurs within a 100 keV wide region centered at 661.6 keV and represents ^{137}Cs primary photons that reached the detector without being attenuated in the medium and that were completely absorbed in the crystal. The broadening of this peak is due to the light flash brightness distribution produced by the scintillation detector, and similar spreading occurs at all energies in the spectrum. A distinguishable feature to the left of the ^{137}Cs peak is a "shelf" occurring below 477.3 keV (the maximum energy that a photon can transfer to an electron in a single Compton-scattering event). Since there is a continuum of electrons up to this energy, the small peak at the shelf edge is located slightly below 477.3 keV after broadening, as shown in Figure 15. Further left along the spectrum is a peak that represents ^{137}Cs photons Compton scattered off the back of the detector vault and then absorbed by the detector crystal. The energy of these photons is equal to 184.3 keV, the difference between 661.6 keV (the initial photon energy) and 477.3 keV (the energy required to Compton scatter a photon 180°, which is the maximum energy that can be imparted to an electron). Finally, to the right of the ^{137}Cs peak is a region representing two-photon processes, and the peak at 1323.2 keV (twice 661.6 keV) represents two 661.6 keV photons being absorbed in the crystal simultaneously.

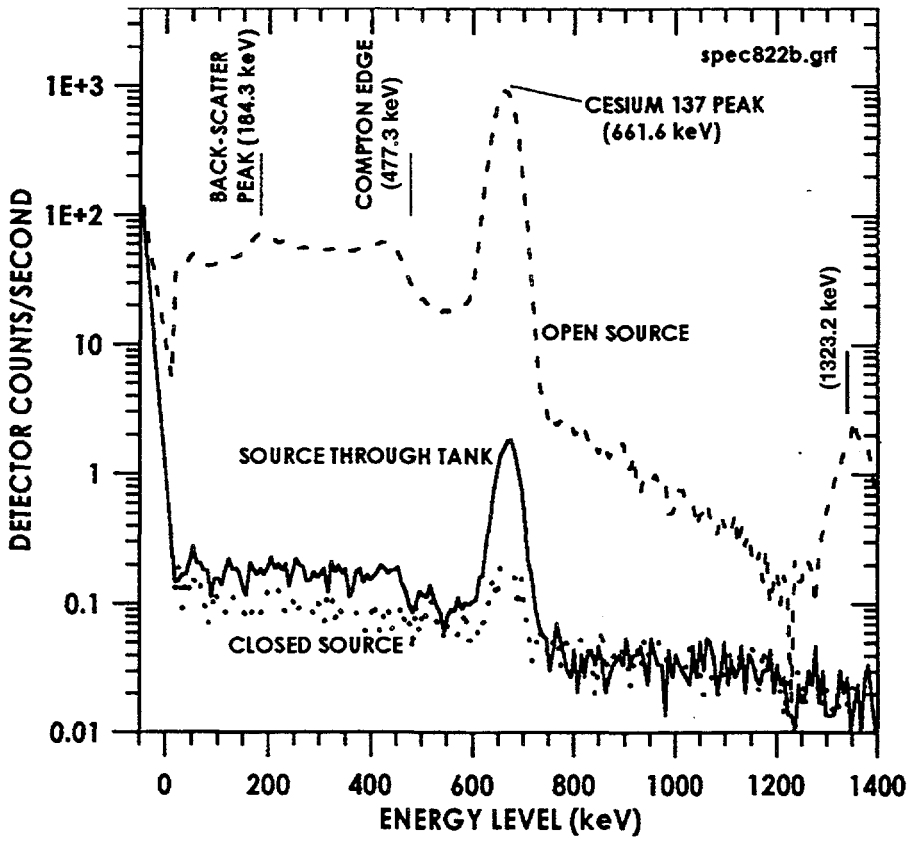

Figure 15. Gamma spectrum from the MCA with various features identified.

It is essential to recognize that the spectra shown in Figure 15 do not represent either the spectrum emitted by the source or the spectrum produced by passage of 661.6 keV photons passing through the testbed being scanned. Rather, the spectra result from the interaction of the 661.6 keV photons with the detector crystal. A 661.6 keV photon interacts with an atom of the detector crystal via Compton scattering or photoelectric absorption. Both of these interactions cause the ejection of one high-energy electron. For photoelectric absorption, this electron acquires all of the photon's energy, and the photon disappears. However, for Compton scattering, the electron acquires only a portion of the photon's energy, and the photon retains the remainder. This lower-energy photon travels in a different direction and can experience further interactions with the crystal. The larger the crystal, the more likely it is that the photon will ultimately experience photoelectric absorption and thus give up all of its energy to electrons. This effect is enhanced by the fact that photoelectric absorption is favored at low energies compared with Compton scattering, which is favored at 661.6 keV. The high-energy electrons lose their energy while passing through the crystal by exciting atoms, which then emit visible light as they return to their ground state. All of these interactions occur almost instantaneously, so a single light flash is observed per incident gamma photon. This light flash is detected and converted into a corresponding voltage by the PMT.

Unfortunately, the brightness of the light flash is related to the energy transferred from the photon to the crystal but cannot be used directly to infer the energy of the incident photon because even monoenergetic incident photons produce light flashes of significantly different brightness. To produce

a light flash corresponding to a photon transferring all 661.6 keV of its energy to the crystal, the sequence of interactions must be terminated within the crystal by a photoelectric absorption. If, however, a Compton-scattered photon escapes from the crystal prior to photoelectric absorption, the light flash corresponds to the energy difference between the incident photon and the escaping photon. For photons experiencing exactly one Compton-scattering event prior to escaping, these energies form a continuum from zero up to the maximum energy a photon can transfer to an electron in a single scattering event (477.3 keV for a 661.6 keV photon). This portion of the spectrum is called the Compton "shelf" or continuum. If a photon experiences more than one Compton-scattering event but escapes from the crystal, a light flash corresponding to an energy between 477.3 keV and 661.6 keV is produced a certain fraction of the time. These effects are mitigated by using a crystal large enough to ensure that most photons deposit all of their energy in the crystal. However, even if all photons transferred identical amounts of energy to the crystal, the resulting light flashes would still not have the same brightness. Rather, a brightness distribution results, with a deviation of roughly 9% about the average for NaI(Tl) crystals. Moreover, if two photons enter the crystal almost simultaneously, the combined light flashes often indicate an energy larger than 661.6 keV.

Count-rate spectra acquired using the MCA must be post-processed to yield the count rate corresponding to the unattenuated 661.6 keV photons from ^{137}Cs. This count rate and the exponential relation for attenuation yield the desired path-averaged attenuation coefficient, as needed for GDT. As discussed above, the observed spectrum is produced almost solely by 661.6 keV photons interacting with the sodium iodide crystal. More specifically, most of the counts at significantly different energies do not indicate that photons of these energies are present in the incident spectrum, which is nearly monoenergetic, or in the transmitted spectrum, which results from the incident spectrum passing through the testbed being scanned. Without a detailed knowledge of the precise form of the spectrum, however, it is impossible to predict rigorously the true number of counts for a spectrum. Initially, summation over a prescribed, fixed "window" of the energy spectrum was examined as a method of determining the count rate. This method, while conceptually simple and straightforward to implement, was not found to produce reliable results during validation experiments, particularly for cases with large attenuation. Subsequently, an approach was developed based on assuming that the spectrum is reasonably described by a Gaussian function in the vicinity of the peak (Knoll, 1979). A curve fit determines the best values for the center, the width, and the height of the Gaussian, and the count rate is determined from the analytical formula for the integration of a Gaussian. To perform the fit, it is necessary to select a fitting window, where only points of the spectrum within the window contribute to the fit. This window is determined adaptively from the measured spectrum so as to contain the 661.6 keV peak and the region around it. Of course, the accuracy of the fit, and hence of the count rate, relies on selecting an appropriate fitting window. However, this is not a particularly severe requirement since the fitting window is used only to determine the Gaussian and not to perform the integration. The above algorithm has been implemented in both Mathematica (Wolfram, 1996) and Fortran to verify its efficacy and was subsequently interfaced with the Labview data acquisition software and has the following steps.

1. Find the maximum count rate per energy bin for all bins in the vicinity of the 661.6 keV peak and the precise bin at which this maximum occurs.

2. Define left and right count-rate cutoff values (e.g. 70% and 10% of the maximum).

3. Find the first bin to the left of the peak where the count rate falls below the left count-rate cutoff and the first bin to the right of the peak where the count rate falls below the right count-rate cutoff. These bins define the fitting window.

4. Take the logarithm of the portion of the spectrum lying within this fitting window, and fit the logarithmic spectrum with a parabola:

$$\ln(dI/dB) = k_0 + k_1 B + k_2 B^2,\ k_2 < 0, \tag{10}$$

where B is the energy bin number, dI/dB is the count rate in energy bin B, and the k_i are the fitting coefficients.

5. The peak center B_p, the peak height I_h, the peak width B_w, and the peak area I (the detector count rate) are given by the following formulas for a Gaussian:

$$B_p = \frac{k_1}{2k_2},\ I_h = \exp(k_0 + k_1 B_p + k_2 B_p^2),\ B_w = \sqrt{\frac{-\pi}{k_2}},\ I = I_h B_w. \tag{11}$$

A series of experiments was performed to validate the use of the MCA for GDT. The experiments consisted of measuring gamma spectra for transmission through various thicknesses of water. Lexan tanks with square inner cross sections of 10.16 × 10.16 cm (4.0 × 4.0 inch) and with inner lengths of 2.54, 5.08, 7.62, 10.16, 12.70, 15.24, and 30.48 cm (1.0, 2.0, 3.0, 4.0, 5.0, 6.0, and 12.0 inch) were used to contain the water. Two tanks were placed in series to extend the path length through water up to 45.72 cm (18 inch). Two combinations of source and detector collimators were used in these experiments: collimator diameters of 6.35 mm (0.25 inch) on both the source and the detector, and collimator diameters of 3.66 mm (0.144 inch) on the source and 3.175 mm (0.125 inch) on the detector. Spectra were always collected for a live time of 60 s. Figure 16 shows some of the gamma spectra measured using the MCA. The different curves in the plot represent different thicknesses of water between the source and detector, in 15.2 cm (6 inch) multiples. The previously discussed features of the spectra are clearly seen in these results. Note that, as the path length is increased, the attenuation above 661.6 keV is roughly double the attenuation below 661.6 keV, which confirms that the spectrum above 661.6 keV results from simultaneous absorption of two gamma photons.

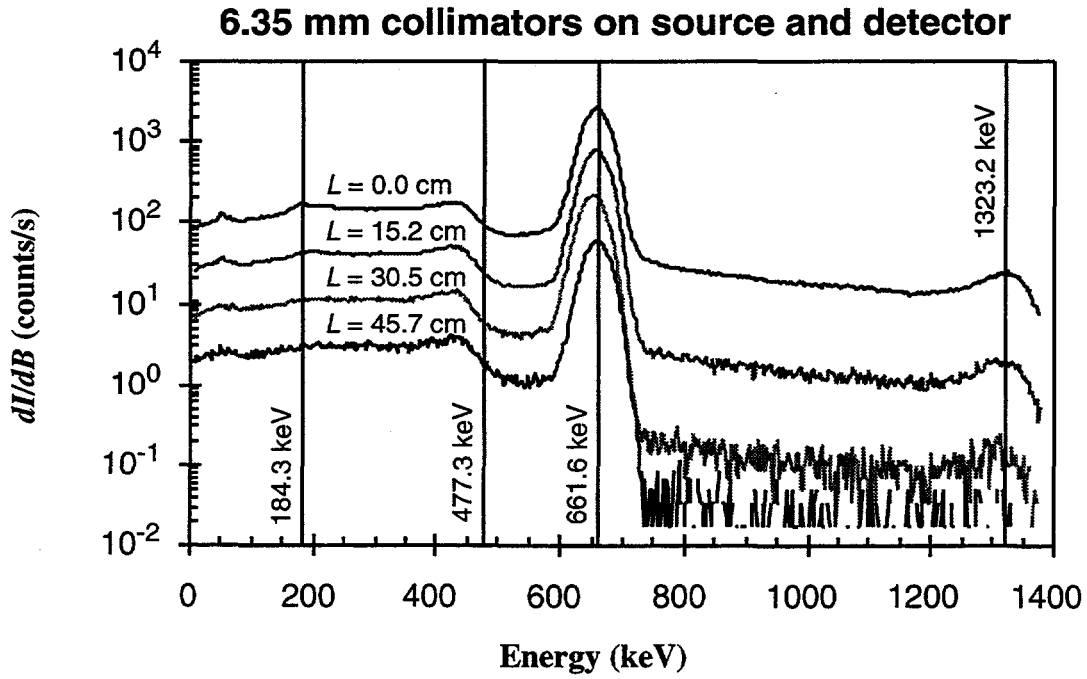

Figure 16. Gamma spectra from the MCA with various thicknesses of water.

The results of applying the algorithm discussed above to the data set shown in Figure 16 are shown in Figure 17. The fits are seen to be very good in the vicinity of the peaks regardless of the peak location or height, and the same fit quality is observed for all other data sets (not shown). Left and right cutoff values of 70% and 10% were used to determine the fitting window. Values of 60-80% for the left cutoff and 10-30% for the right cutoff gave almost identical results, but values of 50% for both cutoffs produced a fit that badly misrepresented the peak. The attenuation coefficient for water was determined to be $\mu_w = 0.0858 \pm 0.0002$ cm^{-1}, in close agreement with the known value (cf. Lamarsh, 1983). A related effort determined the attenuation coefficient of Lexan to be approximately 0.0917 ± 0.0010 cm^{-1}, which appears to be reasonable based on its presumed elemental composition.

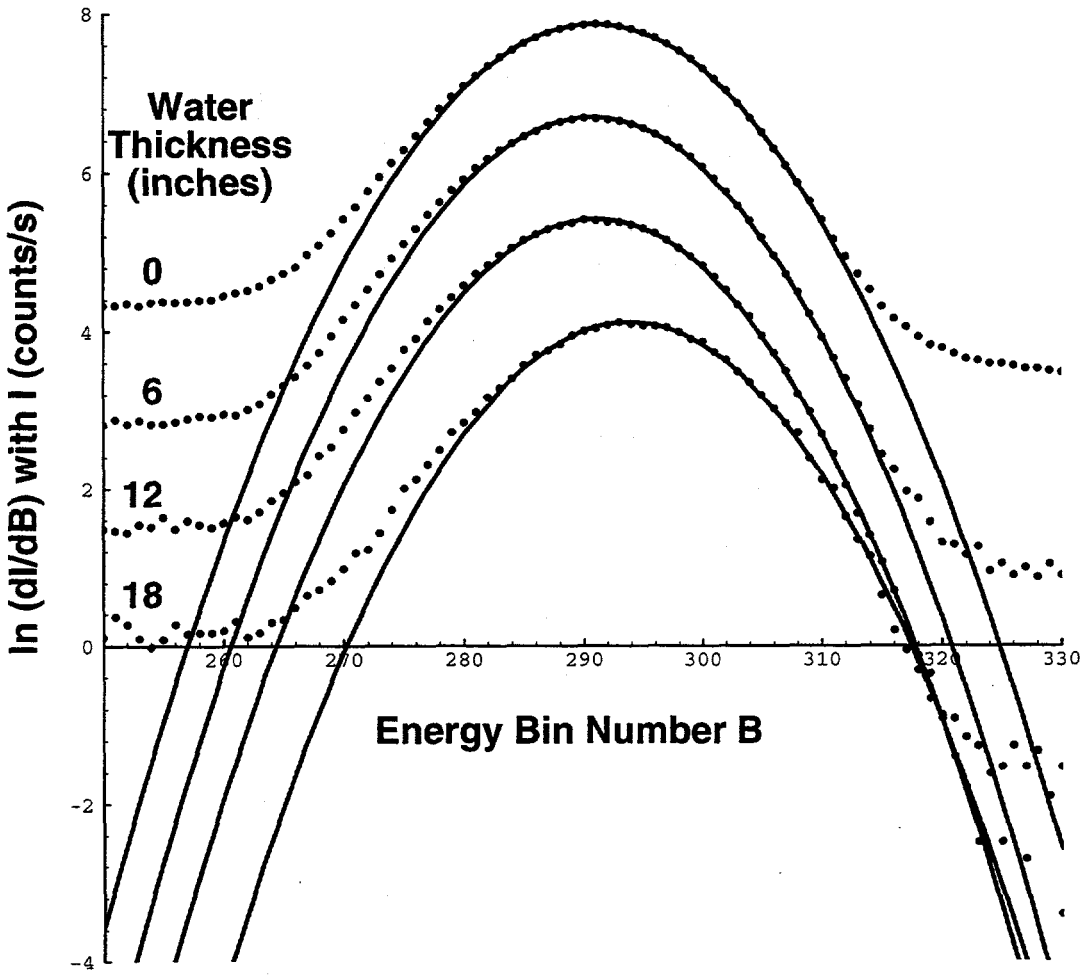

Figure 17. Logarithmic gamma spectra (points) and peak-fitting algorithm (curves).

The fact that the detector cannot respond infinitely fast has implications for data interpretation. If τ is the time required to "detect" a single gamma photon, measurements of count rates comparable to or exceeding $1/\tau$ will not yield accurate results (Reda et al., 1981). Reda et al. (1981) indicate that, for a real count rate I, the measured count rate is given by $I/(1+\tau I)$. For the detection system discussed above, it appears that $\tau \leq 0.5$ μs, indicating that count rates below 20,000 counts/s are measured with better than 1% accuracy.